Polymer 252 (2022) 124943

Contents lists available at ScienceDirect

Polymer

journal homepage: www.elsevier.com/locate/polymer

Tailoring physicochemical properties of collagen-based composites with ionic liquids and wool for advanced applications

Mireia Andonegi [a], Daniela M. Correia [b,c], Carlos M. Costa [b,d,e], Senentxu Lanceros-Mendez [f,g,**], Koro de la Caba [a,f,*], Pedro Guerrero [a,f,h]

[a] BIOMAT Research Group, University of the Basque Country (UPV/EHU), Escuela de Ingeniería de Gipuzkoa, Plaza de Europa 1, 20018, Donostia-San Sebastián, Spain
[b] Physics Centre of Minho and Porto Universities (CF-UM-UP), University of Minho, 4710-057, Braga, Portugal
[c] Centre of Chemistry, University of Trás-os-Montes e Alto Douro, 5000-801, Vila Real, Portugal
[d] Institute of Science and Innovation for Bio-Sustainability (IB-S), University of Minho, 4710-053, Braga, Portugal
[e] Laboratory of Physics for Materials and Emergent Technologies, LapMET, University of Minho, 4710-057, Braga, Portugal
[f] BCMaterials, Basque Center for Materials, Applications and Nanostructures, UPV/EHU Science Park, 48940, Leioa, Spain
[g] Ikerbasque, Basque Foundation for Science, 48009, Bilbao, Spain
[h] Proteinmat Materials SL, Avenida de Tolosa 72, 20018, Donostia-San Sebastián, Spain

ARTICLE INFO

Keywords:
Native collagen
Dielectric response
Antistatic behaviour

ABSTRACT

Wool, choline dihydrogen phosphate ([Ch][DHP]) or choline serinate ([Ch][Seri) ionic liquids (ILs) were incorporated into native collagen formulations and films were prepared by compression molding. Scanning electron microscopy (SEM) images showed no agglomeration, indicating good dispersion of additives within films. The denaturation peak observed by differential scanning calorimetry (DSC), along with infrared spectroscopy (FTIR) results, showed that collagen fibrillary structure was preserved in all samples. These outcomes were correlated with X-ray diffraction (XRD) patterns. Wool or ILs addition increased tensile strength and improved electrical conductivity and all films showed antistatic behaviour. The samples showed a high dielectric constant, mainly determined by mobile charge contributions. This work shows the potential of native collagen films with tuneable physical-chemical characteristics for a new generation of sustainable materials for a wide variety of applications.

1. Introduction

Smart and multifunctional materials are becoming the base of rapid developments in areas such as sensors and actuators, energy storage and harvesting, wearable electronic devices, and biomedical applications, among others [1,2]. In particular, smart materials are characterized by a controllable, specific and reproducible response to specific stimuli, such as electric and magnetic fields, temperature or pressure [3].

Apart from technical properties and behavioural characteristics, sustainability is becoming increasingly demanded in this field. For this reason, natural and renewable polymers are gaining increasing attention as a suitable alternative to develop the next generation of smart materials [4]. Among the different natural polymers, collagen has been extensively studied due to its availability as well as structural and functional roles. Collagen is the most abundant protein of the extracellular matrix (ECM) in vertebrates [5]. It consists of three parallel polypeptide-alpha chains in a right-handed triple-helical structure, which self-associates to form highly ordered cross-linked fibrils. Those fibrils, in turn, form insoluble fibres providing the extracellular matrix with a high integrity and mechanical tensile strength due to the tight winding triple helix structure [6]. Hence, collagen-based materials have appeared in a number of applications, for example wound dressings, due to their non-immunogenicity and poor antigenicity and, thus, biocompatibility [7]. Furthermore, collagen takes part in tissue regulation, growth and repair, due to its capacity to act as a substrate for cell adhesion and growth [8,9].

Additionally, the polar character of collagen provides interesting electrical properties. Collagen triple helical structure is stabilized by

* Corresponding author. BIOMAT Research Group, University of the Basque Country (UPV/EHU), Escuela de Ingeniería de Gipuzkoa, Plaza de Europa 1, 20018, Donostia-San Sebastián, Spain.
** Corresponding author. BCMaterials, Basque Center for Materials, Applications and Nanostructures, UPV/EHU Science Park, 48940, Leioa, Spain.
E-mail addresses: senentxu.lanceros@bcmaterials.net (S. Lanceros-Mendez), koro.delacaba@ehu.eus (K. Caba).

https://doi.org/10.1016/j.polymer.2022.124943
Received 12 February 2022; Received in revised form 18 April 2022; Accepted 5 May 2022
Available online 10 May 2022

hydrogen bonds between carbonyl and hydroxyl groups of hydroxyproline residue [10]. These hydrogen bonds, together with electrostatic interactions, not only stabilize the protein structure, but also contribute to the electrical properties of collagen. Hence, due to a change in the redistribution of electrical charges, when the material is exposed to an electric field, collagen is a polarizable material [11].

Notwithstanding the potential electrical properties, relatively few dry collagen electrical conduction experiments have been carried out. Bardelmeyer [12] measured the electrical conductivity of bovine Achilles tendon with various amounts of adsorbed water as a function of temperature. These authors concluded that the conduction appeared to be fully determined by the hydration water. Therefore, the electrical properties of proteins, in general, depend on the stable dipole moments associated with water molecules, being higher the conductivity when higher is the number of dipoles [13]. Furthermore, regarding their sensitivity to environmental factors such as water vapour and carbon dioxide, collagen can be used as bio-sensor giving a response in terms of resistance, voltage or current [14].

At the same time, in the last two decades, ionic liquids (ILs) have attracted considerable attention in many fields, such as electrochemistry [15], synthesis [16], catalysis [17] and material science [18]. ILs consist of salts composed by different combinations of organic cations and organic or inorganic anions [19], which show a melting temperature below 100 °C, non-flammability, negligible volatility, high ion conductivity, and thermal, electrochemical and chemical stability [20]. Here, the combinations of a polymer with ILs offer new opportunities in polymer materials science and, in particular, they seem to be promising candidates as new materials for multifunctional applications [21,22].

The flexibility in the molecular design of ILs allows the design and synthesis of a large variety of ILs with specific functionalities. However, conventional ILs like imidazolium, phosphonium and ammonium based ILs demonstrated destabilization effect at the higher structural hierarchical level of collagen, poor biodegradability, and low biocompatibility [23–25]. In this context, biocompatible ILs (bio-ILs) have emerged to meet the need to develop more environmental-friendly ILs and prevent the associated toxicity issues. Choline based ILs and choline aminoacid-based ILs, such as choline dihydrogen phosphate ([Ch][DHP]) and choline serinate ([Ch][Seri]), belong to the biocompatible ILs (bio-ILs) family [26]. Both bio-ILs have stabilizing effect on collagen structure by exerting an electrostatic force and acting as crosslinker, which together with their biocompatibility lead to a variety of applications in drug delivery and sensor development [27].

Additionally, wool fibber is a multicomponent fibber consisted of 170 different protein molecules distributed in three main morphological components: cuticle, cortex, and cell membrane complex. The surface consists of overlapping cuticles, surrounded by lanonin (waxy substance). The cortex is formed by cortical cells and it is the responsible of putting the crimp in wool. Finally, the membrane is formed by keratin molecules self-assembled in α-helix secondary structure. Keratin chains are self-associated to form highly organized microfibrils and macrofibrils [28]. Keratin comprises up to 95% by weight of wool and exhibits a high degree of chemical functionalities, including amide, carboxyl, sulfoxide, and sulfide, among others [29]. In this sense, wool has been widely used in textiles and various technological fields due to its fibrillary structure, high moisture regain, resiliency, good elasticity, electrical insulation characteristics, and low heat conductivity, among others [30]. Furthermore, large amount of wool waste is generated annually, which become a critical issue, due to social and environmental concerns [31]. Although several reports have recently shown the potential of collagen-keratin composites, especially in biomedical applications [32–34], no reports have been done about wool-collagen composites for non-textile applications. Therefore, collagen films with two different wool contents were prepared in this work to analyse the effect of this fibrillary additive on the structure and properties of collagen films.

In this context, the aim of this study was the assessment of the incorporation of [Ch][DHP], [Ch][Seri] and wool into collagen formulations to prepare films by compression moulding in order to improve mechanical and electrical properties of collagen and relate them with physicochemical properties and the changes in collagen structure. Thus, the objective of this work was to determine the potential applicability of these materials in electronics, sensors and actuators, among others.

2. Materials and methods

2.1. Materials

Bovine collagen from trimmings and the splitting-derived residues, with 33% glycine, 22% imino acids, 12% proline, 11% alanine and 10% hydroxyproline, was supplied by Tenerias Omega (Spain). Wool from latxa sheep was supplied by Landazurieta farm in Ametzaga de Zuia (Alava). [Ch][DHP] (>98%) and [Ch][Seri] (>95%, 60% in H_2O) were supplied by Ionic Liquids Technologies GmbH (Germany). Glycerol (pharma grade with a purity of 99.01%), used as plasticizer, and acetic acid were supplied by Panreac Quimica S.L.U (Barcelona, Spain).

2.2. Samples preparation

2.2.1. Collagen treatment

Native collagen was obtained according to the method reported by Andonegi et al. (2020). Firstly, bovine skins were defatted by immersion into 1 M NaOH solution for 12 h and neutralized by immersion into phosphate buffer saline (PBS) solution (pH 7.4). Then, collagen was grinded and freeze-dried in order to facilitate the subsequent processing.

2.2.2. Wool treatment

In order to remove impurities, wool fibres were washed twice at room temperature with tap water and soap (pH 7), and dry in an oven at 30 °C for 48 h before being used.

2.2.3. Mixture preparation

After wool and collagen treatments, collagen mixtures were prepared with wool or IL. For that, 0.1 wt % [Ch][DHP], 0.1 wt % [Ch][Seri], 5 wt % wool or 10 wt % wool (all additives on collagen dry basis) were used. Collagen, additives, 20 wt % glycerol (based on dry collagen) and 0.5 M acetic acid (1:2 collagen/acetic acid ratio) were mixed using a T25 ultraturrax IKA (Barcelona, Spain) in a cold bath to prevent the dough from heating up, until homogeneous pastes were achieved (2000 rpm, 2 min). These pastes were used for rheological tests and for film preparation by compression moulding.

2.2.4. Rheological evaluation

The viscoelastic properties of collagen mixtures were studied at 35 °C with a Thermo Scientific Haake Rheostress1 Rheometer (Vigo, Spain), equipped with a 35 mm diameter serrated plate-plate geometry and a gap between plates of 1 mm. Firstly, strain sweep tests were carried out between 0.01% and 100% strain at a constant frequency of 1 Hz to determine the linear viscoelasticity region (LVR) and the critical strain of LVR. Subsequently, temperature sweeps were carried out from 35 °C to 70 °C to obtain elastic (G') and viscous (G") moduli, as well as the complex viscosity (η*), with the frequency fixed at 1.0 Hz and the strain at 1%.

2.2.5. Film preparation

The hydrated doughs were moulded by hot-pressing in a Specac press (Barcelona, Spain). The dough was placed between two aluminium plates, previously heated up to 50 °C for 30 s, and then pressed at 0.5 MPa for 1 min to obtain the films. It is worth noting that those temperature and pressure conditions were selected since no film could be obtained at lower temperatures. Films with thickness between 20 and 30 μm, measured with QuantuMike digimatic micrometer Mitutoyo (Elgoibar, Spain), were obtained. Films were designated as control

(pristine collagen film), 5wool (sample with 5 wt % wool), 10wool (sample with 10 wt % wool), 0.1 [Ch][DHP] (sample with 0.1 wt % [Ch][DHP]), and 0.1 [Ch][Seri] (sample with 0.1 wt % [Ch][Seri]) as a function of the additive type and content. Films were conditioned at 25 °C and 50% relative humidity in an ACS Sunrise 700 V bio-chamber (Madrid, Spain) for 48 h before testing, when moisture content values were measured: 20.0 ± 0.8% for control films, 14.0 ± 0.5% for 0.1 [Ch][DHP] and 0.1 [Ch][Seri] films, and 12.0 ± 0.6% for 5wool and 10wool films.

2.3. Samples characterization

2.3.1. Differential scanning calorimetry (DSC)

DSC measurements were performed by a Mettler Toledo DSC 822 (Madrid, Spain). Samples (3 mg) were sealed in aluminium pans to prevent mass loss and subjected to a heating ramp from −50 °C to 250 °C at a rate of 10 °C/min under nitrogen atmosphere (10 mL N_2/min) to avoid oxidation.

2.3.2. Fourier transform infrared (FTIR) spectroscopy

FTIR spectra were performed by using a Nicolet 380 FTIR spectrometer (Madrid, Spain) equipped with attenuated total reflectance (ATR) crystal (ZnSe). FTIR spectra were obtained from 4000 to 800 cm^{-1}. A total of 32 scans were carried out at 4 cm^{-1} resolution.

2.3.3. Water uptake (WU)

Rectangular pieces of 1 cm × 2 cm were weighed (w_i), and then immersed into PBS (pH 7.4) in order to maintain the solution pH constant. After specific times, the samples were taken out, wiped, weighed (w_f), and immersed into PBS again until constant values were achieved. WU was calculated as follows:

$$WU\ (\%) = \frac{w_f - w_i}{w_f} x\ 100 \tag{2}$$

2.3.4. X-ray diffraction (XRD)

XRD was performed with a PANalytical Xpert PRO diffraction unit (Madrid, Spain), operating at 40 kV and 40 mA. The radiation was generated from a Cu-Kα (λ = 1.5418 Å) source. The diffraction data were collected from 2θ values from 2 to 50°, where θ is the angle of incidence of the X-ray beam on the sample.

2.3.5. Scanning electron microscopy (SEM)

A Hitachi S-4800 scanning electron microscope was used (Barcelona, Spain). Prior to observation, samples were mounted on a metal stub with double-side adhesive tape and coated under vacuum with gold, using a JEOL fine-coat ion sputter JFC-1100, in an argon atmosphere. All samples were examined using an accelerating voltage of 15 kV.

2.3.6. Mechanical properties

Tensile strength (TS) and elongation at break (EAB) were measured at room temperature, using a Linkam Scientific Instruments TST 360 (Barcelona, Spain). Specimens were cut into rectangular-shaped samples of 30 mm × 10 mm and tensile tests were performed at a constant deformation of 50 μm s^{-1} and with a load cell of 20 N.

2.3.7. Electrical and dielectric properties

The DC volume electrical conductivity (σ, S/cm) of the samples was obtained after measuring the characteristic I–V curves at room temperature with an applied voltage between ± 10 V using a Keithley 487 picoammeter/voltage source (Barcelona, Spain). Previous to the measurements, the samples were coated on both sides with 5 mm circular diameter electrodes and σ was calculated by:

$$\sigma = \frac{d}{R.A} \tag{3}$$

where d is thickness, R is the resistance of the sample, and A is the electrode area.

Dielectric measurements were performed using a Quadtech 1920 LCR precision meter. The capacity and tan δ were obtained at room temperature in the frequency range of 1 kHz to 1 MHz with an applied voltage of 0.5 V. Then, the real part (ε') of the dielectric function and tan δ were obtained:

$$\varepsilon' = \frac{C.d}{\varepsilon_0.A} \tag{4}$$

$$tan\ \delta = \frac{\varepsilon''}{\varepsilon'} \tag{5}$$

where C is the capacitance (F), ε_0 is the permittivity of vacuum (8.85×10^{-12} F m^{-1}), A is the electrode area (m^2) and d is the thickness of the sample (m).

The AC electrical conductivity was calculated by equation (6):

$$\sigma'(\omega) = \varepsilon_0 \omega \varepsilon''(\omega) \tag{6}$$

where ε_0 is the permittivity of free space, $\omega = 2\pi f$ is the angular frequency and $\varepsilon''(\omega) = \varepsilon'\ tan\ \delta$ is the frequency dependent imaginary part of the dielectric permittivity.

2.3.8. Statistical analysis

Analysis of variance (ANOVA) was carried out with SPSS software (SPSS Statistic 25) to determine significant differences between samples. Tukey's test with a statistically significance at the $P < 0.05$ level was considered for multiple comparisons among different systems.

3. Results and discussion

3.1. Rheological behaviour

Compression moulding is a processing method in which the raw material is summited to a determined pressure and temperature for a specific period by using a metal mould, in order to obtain the final product with a specific shape [35]. In this sense, it is of great relevance to determine the minimum processing temperature at which collagen flows while preserving its native structure [36]. Therefore, the thermo-rheological behaviour of the control sample was analysed by performing temperature sweep tests in oscillatory shear. As can be observed in Fig. 1, G′ was greater than G'' at room temperature and, thus, the sample showed a predominant elastic behaviour due to the limited molecular free motion [37]. As the temperature increased, the

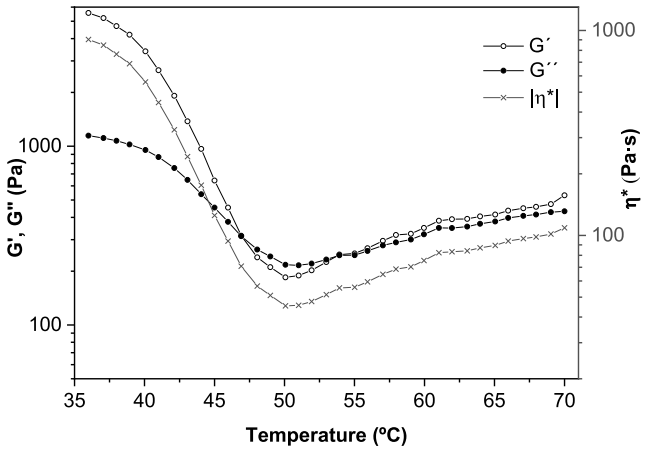

Fig. 1. Storage moduli (G′), loss moduli (G''), and complex viscosity (η*) of the control film as a function of temperature.

storage and loss modulus, as well as the complex viscosity (η*), decreased down to a minimum value at 50 °C, demonstrating a large influence of temperature on the collagen structure. This decrease of η* with temperature was related to the motion of collagen chains caused by the breakage of hydrogen bonds of free and bound water, as can be observed by the first endothermic peak of the DSC curves (Fig. 2). In this regard, the effect of temperature on the rheological properties of collagen solutions has been analysed [38,39] and defined the transition observed at 25–39 °C as collagen denaturation temperature. However, taking into consideration that the thermal denaturation depends strongly on the degree of hydration [36], collagen was minimally hydrated in this work to be processed at low temperature and avoid collagen denaturation. Furthermore, it is worth nothing that the viscous behaviour predominated within the temperature range of 47–53 °C, since G'' was slightly higher than G′ and, thus, this represented the optimum temperature range to process collagen by compression moulding.

3.2. Thermal and physicochemical properties

While rheological properties provide information about the sample processability, thermal properties provide information about the effective temperature limits at processing conditions and the effect of manufacturing processes on collagen structure [40]. Therefore, DSC analysis was carried out and results are shown in Fig. 2.

It can be observed that all samples exhibited the characteristic endothermic peaks of collagen: the first peak, around 75–80 °C, was related to free and bound water release [41]; and the second phase transition, around 122–138 °C, was associated to the denaturation of native collagen triple helix and, simultaneously, to the structural water release [42].

It is worth noting that collagen can denature depending on the processing temperature, but the hydration of the samples must also be considered. When collagen is prepared in solution, denaturation temperature is around 40 °C [43]. However, collagen with relatively low hydration shows denaturation temperatures higher than 150 °C [44]. Therefore, due to the conditions used for compression moulding in this work (50 °C for 90 s) and the hydration level (1:2 collagen/acetic acid ratio), it can be said that denaturation did not occur during processing. Furthermore, DSC thermograms (Fig. 2) show the denaturation peak for all samples. This denaturation peak also appeared when the additives were incorporated, indicating the maintenance of the triple helix structure after compression moulding, even if the peak appeared at lower temperatures, 126 °C for the films with ILs and 10wool and 122 °C for 5wool. It can be noted that the height of the first peak decreased when the additives were incorporated, probably due to the difference on moisture content of the samples [45].

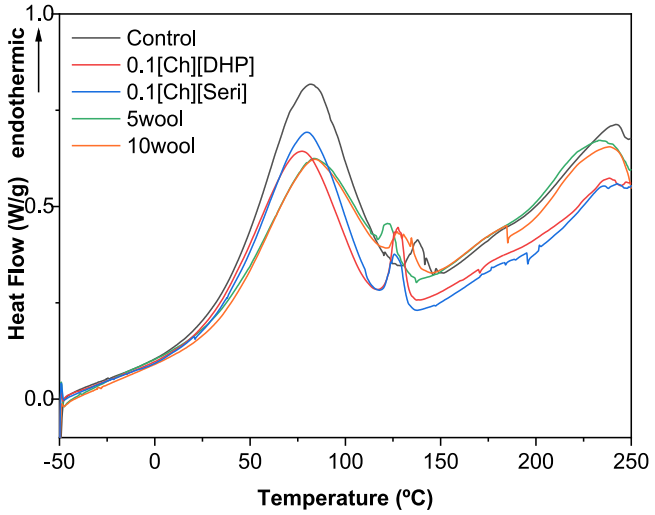

Fig. 2. DSC thermograms of all collagen-based films.

In order to assess the interactions among the components of the films, FTIR analysis was carried out and the spectra are exhibited in Fig. 3a. All the spectra showed the characteristic absorption bands assigned to the peptide bonds in collagen: amide I (C═O stretching), amide II (N–H bending) and amide III (C–N stretching) observed at 1632, 1540, and 1239 cm^{-1}, respectively [46,47]. A slight decrease in the intensity of amide I, II and III bands by the addition of the ILs may indicate physical interactions between the components of the samples, i.e. between the anion and cation of the ionic liquids and the carboxyl, amino and hydroxyl groups of collagen and glycerol. Additionally, when wool was added, a slight decrease in the intensity of the amide bands was observed, suggesting physical interactions among carboxylic, amine and hydroxyl group in collagen with the carboxylic and amine groups of the keratin in wool and the hydroxyl groups of glycerol. Although the hydrocarboxylic radical of choline cation in ILs and phosphorus dioxide group in 0.1 [Ch][DHP] should be perceived at 1065 and 946 cm^{-1} [48], these bands were overlapped by the characteristic bands of glycerol in the region of 850–1000 cm^{-1}. Similarly, the disulphide linkages of keratin in wool should appear in the region of 998–1100 cm^{-1} [49].

Additionally, water uptake tests were carried out and the results are shown in Fig. 3b. In the first 10 min of immersion, the water uptake values increased rapidly due to the low thickness of the samples. After 60 min of immersion, the equilibrium values were achieved at around 375% for control films and 325% for the films with ILs or wool. These different water uptake values suggested that the incorporation of both ILs types or wool promoted the interactions with the polar groups of collagen and glycerol. As a consequence, polar groups were less accessible to interact with water molecules and, thereby, a lower water uptake degree was achieved. Furthermore, the more compact structure of the samples with ILs or wool, observed by SEM analysis (Fig. 4), may decrease the water uptake values as well. It is also worth noting that no significant differences were observed between the water uptake values of the films with ILs or wool.

3.3. Morphological and structural characteristics

The effect of ILs or wool on collagen structure was assessed by SEM and XRD analyses (Fig. 4). Concerning SEM analysis, the micrograph of the cross-section in control films -pristine collagen- (Fig. 4a) exhibited the dense network of collagen fibres. With the addition of ILs or wool (Fig. 4b–e), fibres could not be observed, and a more compact structure was achieved, which could explain the lower water uptake capacity observed in the samples containing ILs or wool (Fig. 3b). It is worth noting that no agglomeration was observed in the samples with ILs or wool, indicating the good dispersion of both ILs and wool within the films.

Regarding XRD analysis (Fig. 4f), all samples showed the characteristic collagen amorphous structure, with a broad peak around 20°, associated with the diffuse scattering of collagen fibres [50]. The first peak around 7° represents the triple helix structure of collagen and the lateral packing distance between collagen chains [51]. When wool was incorporated, a decrease in the intensity of both peaks was observed, indicating a change in the secondary structure of collagen. Additionally, a shoulder around 10° can be appreciated in 5wool and 10wool that may represent the α-helix structure of keratin in wool [52]. It is worth noting that the slight changes observed by FTIR and XRD indicate that the secondary structures of collagen and wool were mostly preserved. Additionally, the incorporation of ILs caused a more noticeable decrease in the intensity of the peak around 20°, suggesting that the structural order in collagen changed. These differences in the structural order of collagen in ILs and wool containing samples may be due to the molecular size of the additives. ILs are smaller and soluble in the solvent used (acetic acid), so that they can penetrate between the collagen chains and

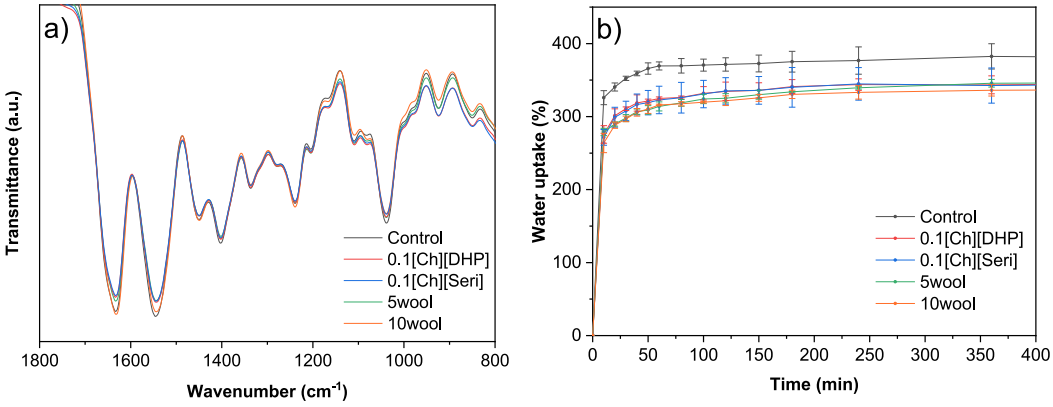

Fig. 3. Physicochemical properties of collagen-based films: a) FTIR spectra from 1800 to 800 cm^{-1} and b) water uptake curves.

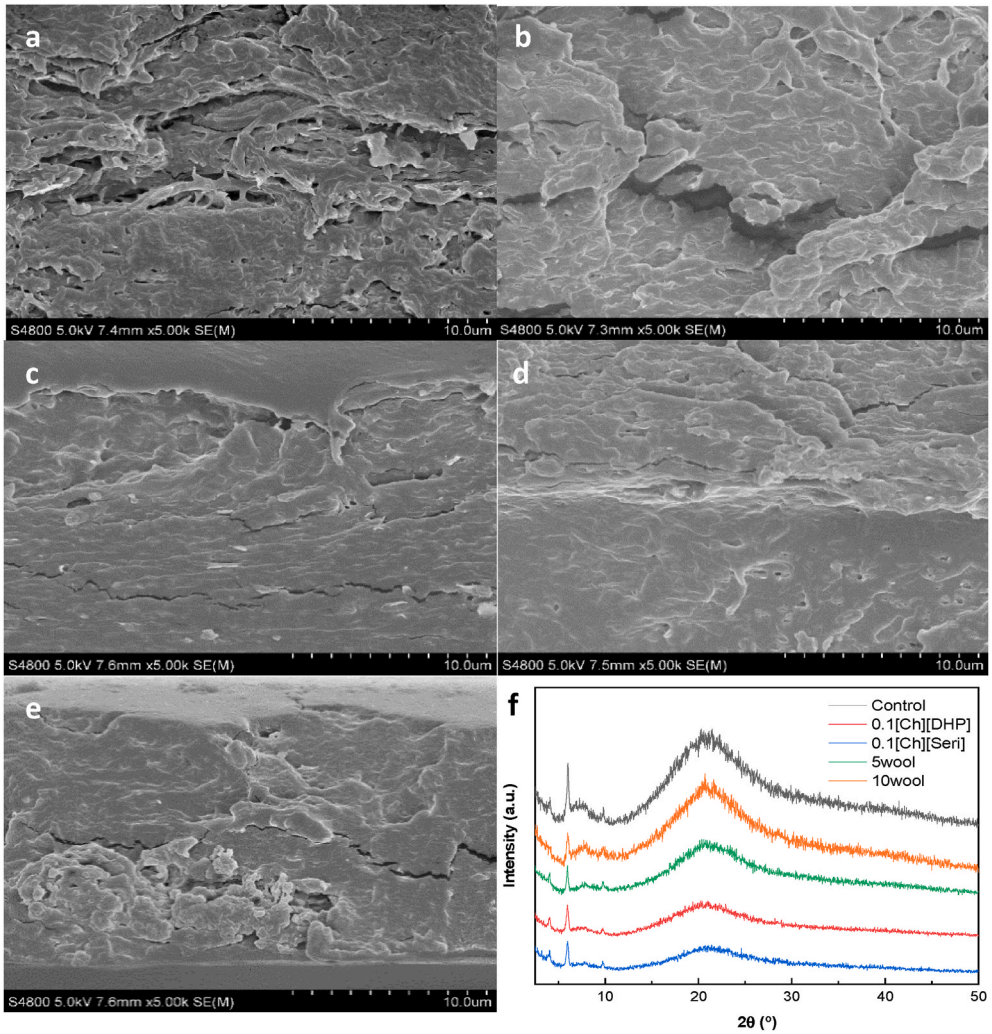

Fig. 4. Morphological and structural properties of collagen films: SEM images of cross-sections (x5000 magnification) for a) control b) 0.1 [Ch][DHP], c) 0.1 [Ch][Seri], d) 5wool, and e) 10wool films, and f) XRD patterns.

can change collagen structural order. In the case of wool, this is not soluble and the fibres are larger so that the secondary structures of collagen and keratin in wool are preserved, and the interactions are lateral interactions between the microfibers of both.

3.4. Mechanical properties

Tensile tests were performed in order to evaluate the effect of ILs or wool addition on the mechanical behaviour of collagen films (Fig. 5). This behaviour is associated to the fibril structure of collagen; as the stress increased, the fibres of collagen were orientated, increasing tensile

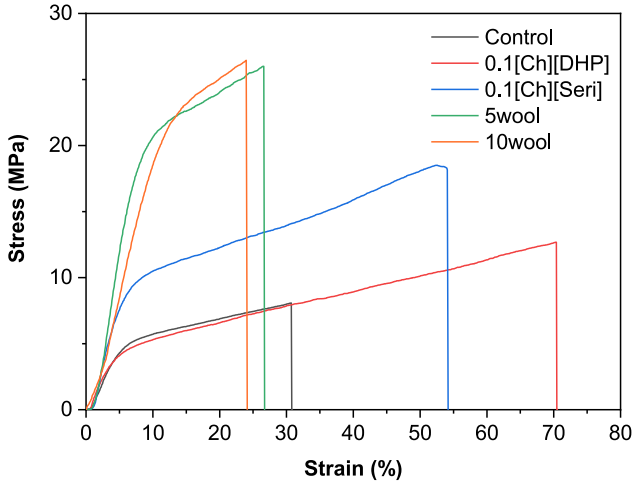

Fig. 5. Stress-strain curves of collagen-based films.

resistance up to the point of break [53].

The values of tensile strength (TS) and elongation at break (EAB) are shown in Table 1. On the one hand, the addition of lLs caused a significant ($p < 0.05$) increase in both TS and EAB values, attributed to the chemical structure of ILs and their role as plasticizers, respectively [54]. On the other hand, when wool was added, EAB decreased ($p < 0.05$), but TS significantly ($p < 0.05$) increased. This behaviour may be attributed to the good compatibility between collagen and wool and to the strong mechanical resistance associated to wool fibres [55]. Although different collagen treatments and processing methods used in the works reported in the literature make comparisons difficult, a similar effect was shown for collagen films with casein [56], where TS values increased from 17.24 MPa to 24.87 MPa and, simultaneously, EAB values decreased from 13.88 to 2.87%.

3.5. Electrical conductivity and dielectric properties

Fig. 6a shows the I–V curves obtained for the pristine collagen film and for the ones reinforced with ILs or wool. The addition of ILs or wool improved the electrical conductivity of collagen. As can be seen in Fig. 6a), the collagen-based films show electrical conductivity values compatible with an antistatic behaviour [57]. The DC conductivity of the pristine collagen film was 2.34×10^{-9} S/cm, and increased with the addition of IL, being 1.03×10^{-9} S/cm for 0.1 [Ch][DHP] and 1.87×10^{-8} S/cm for 0.1 [Ch][Seri] films. This increase is related to the increase of ionic mobile species associated to the IL. When wool was added, the DC electrical conductivity increased with wool addition and content due to the proton conduction. Conduction occurs by proton exchange between the hydroxyl groups of the wool and those related to absorbed water molecules [58]. In this case, a nonlinear behaviour was observed and the peak detected around 3 V was indicative of a variation of the conduction regime -decrease of the electrical conductivity-, related to the effect of absorbed water in wool (hygroscopic behaviour).

Table 1
Tensile strength (TS) and elongation at break (EAB) of the collagen-based films.

Films	TS (MPa)	EAB (%)
Control	7.36 ± 1.13^{a}	31.99 ± 4.68^{a}
0.1 [Ch][DHP]	13.30 ± 0.33^{b}	$68.00 \pm 4.57^{a,b}$
0.1 [Ch][Seri]	18.07 ± 1.16^{c}	57.72 ± 4.57^{b}
5wool	24.39 ± 3.64^{d}	27.25 ± 3.21^{c}
10wool	28.31 ± 2.85^{d}	23.30 ± 1.87^{d}

[a-d]Two means followed by the same letter in the same column are not significantly ($p > 0.05$) different through the Turkey's multiple range test. $n = 5$ was the minimum number of replications.

This effect is reduced after drying, as shown for 5wool films in Fig. 6a (dot line), demonstrating the effect of the hydroxyl groups on proton conduction. Additionally, Fig. 6b) shows the I–V cycling curves for 20 cycles for the pristine collagen films, demonstrating a low hysteresis in the electrical conductivity, which is representative for the rest of the samples.

Fig. 7a) and b) show the dielectric constant (ε') and the loss factor (tan δ), respectively. As the frequency increased, ε′ and tan δ decreased, indicating a slow dynamic of the contributions to the dielectric response, mainly attributed to mobile charge carriers. Furthermore, ε′ and tan δ increased with the addition of ILs and 5 wt % wool due to the fact that these fillers increased the number of charge carriers. Further, the high values of ε′ and, in particular, of tan δ demonstrate conductivity contributions to the dielectric response by the different charge carriers from collagen, wool and IL. As can be seen in Fig. 7c), the conductivity increased with frequency, indicating strong contributions from localized charge carrier mobility. Two regimes in the conductivity behaviour were observed in all films: one regime for medium frequencies up to 10^4 Hz, dominated by the DC conductivity; the second, at higher frequencies, assigned to the AC conductivity. Furthermore, the presence of ILs and 5 wt % wool increased the AC conductivity values compared to the control film due to the increased presence of localized charge carriers, contributing to the electrical response. The electrical results of neat collagen, which depend on several factors such as the soluble state of collagen and collagen concentration, among others, are similar to those observed in the literature [59,60]. Furthermore, collagen films with ILs present a high dielectric constant as a result of the interactions of collagen with ILs, contributing to the electrical response.

4. Conclusions

Advanced functional materials based on native collagen with ILs or wool were successfully prepared by compression moulding, resulting in homogeneous and easy to handle films. The results found by DSC, FTIR, and XRD showed the prevalence of the collagen fibrillar structure in all films after the compression moulding process. Regarding physico-chemical properties, lower water uptake capacity was observed with the incorporation of ILs or wool into the formulations, probably due to the formation of a more compact structure, as shown by the SEM images of film cross-sections. Furthermore, the addition of lLs or wool caused a significant increase in tensile strength and improved the electrical conductivity and dielectric response. The high dielectric response of the samples demonstrated the mobile contributions, highlighting the potential of these collagen films for an antistatic application with a focus on sustainability. In particular, 0.1 [Ch][Seri] films showed the best mechanical and electrical properties, since addition of the IL improved TS, EAB and DC values. Additionally, if materials with higher TS values were needed, the combination of IL with wool in the collagen matrix could be an interesting option to analyse.

Data availability

The raw/processed data required to reproduce these findings cannot be shared at this time as the data also forms part of an ongoing study.

CRediT authorship contribution statement

Mireia Andonegi: Investigation, Writing – original draft. **Daniela M. Correia:** Investigation, Writing – original draft. **Carlos M. Costa:** Conceptualization, Resources, and, and. **Senentxu Lanceros-Mendez:** Resources, Supervision, Writing – review & editing, Funding acquisition. **Koro de la Caba:** and, Supervision, Writing – review & editing, and. **Pedro Guerrero:** and, and, and.

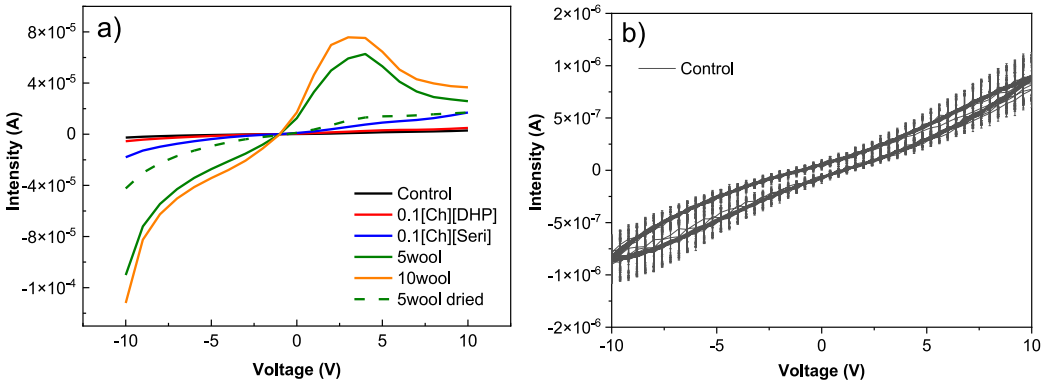

Fig. 6. a) Current-voltage (I–V) curves and b) cycling current-voltage (I–V) curves.

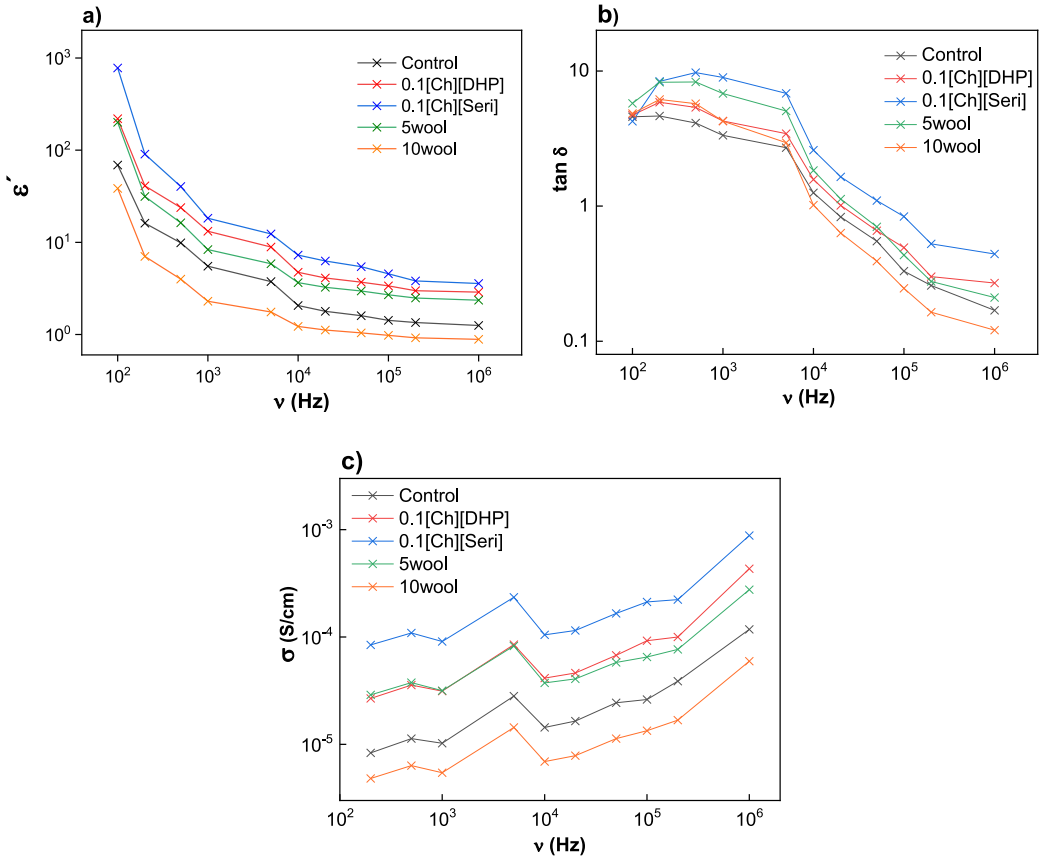

Fig. 7. a) Variation of ε′, b) tan δ and c) AC electrical conductivity values as a function of frequency in a log–log plot.

Declaration of competing interest

The authors declare that they have no known competing financial interests or personal relationships that could have appeared to influence the work reported in this paper.

Acknowledgments

This research was funded by MCI/AEI/FEDER, UE, grant number RTI2018-097100-B-C22. This work was also supported by the Portuguese Foundation for Science and Technology (FCT) under strategic funding UIDB/04650/2020, UID/FIS/04650/2021, project PTDC/FIS-MAC/28157/2017, grant SFRH/BPD/121526/2016 (D.M.C) and Investigator FCT Contract 2020.04028.CEECIND (C.M.C.) funded by national funds through FCT and by the ERDF through the COMPETE2020-Programa Operacional Competitividade e Internacionalização (POCI). The authors also acknowledge funding from the Basque Government (KK-2021/00131). Mireia Andonegi also thanks the Basque Government for her fellowship (PRE_2017_1_0025). Thanks are also due to the Advanced Research Facilities (SGIker) from the UPV/EHU. Finally, the authors would like to thank Paula Menoyo for the wool provided.

References

[1] Q. Rong, W. Lei, M. Liu, Conductive hydrogels as Smart materials for flexible electronic devices, Chem. Eur J. 24 (2018) 16930–16943, https://doi.org/10.1002/chem.201801302.

[2] F.A. Hassani, Q. Shi, F. Wen, T. He, A. Haroun, Y. Yang, Y. Feng, C. Lee, Smart materials for Smart healthcare-moving from sensors and actuators to self-sustained nanoenergy nanosystems, Smart Mater. Med. 1 (2020) 92–124, https://doi.org/10.1016/j.smaim.2020.07.005.

[3] N. Shehata, M.A. Abdelkareem, E.T. Sayed, D.E. Egirani, A.W. Opukumo, Smart materials: the next generation, in: Reference Module in Materials Science and Materials Engineering, 2021, https://doi.org/10.1016/B978-0-12-815732-9.00062-0.

[4] H.C. Kim, S. Mun, H.U. Ko, L. Zhai, A. Kafy, J. Kim, Renewable smart materials, Smart Mater. Struct. 25 (2016), 073001, https://doi.org/10.1088/0964-1726/25/7/073001.

[5] P.C. Balaure, A.M. Holban, A.M. Grumezescu, G.D. Mogoşanu, T.A. Bălşeanu, M. S. Stan, A. Dinischiotu, A. Volceanov, L. Mogoantă, *In vitro* and *in vivo* studies of novel fabricated bioactive dressings based on collagen and zinc oxide 3D scaffolds, Int. J. Pharm. 557 (2019) 199–207, https://doi.org/10.1016/j.ijpharm.2018.12.063.

[6] B. An, Y. Lin, B. Brodsky, Collagen interactions: drug design and delivery, Adv. Drug Deliv. Rev. 97 (2016) 69–84, https://doi.org/10.1016/j.addr.2015.11.013.

[7] A.K. Lynn, I.V. Yannas, W. Bonfield, Antigenicity and immunogenicity of collagen, J. Biomed. Mater. Res. Part B 71B (2004) 343–354, https://doi.org/10.1002/jbm.b.30096.

[8] A.M. Ferreira, P. Gentile, V. Chiono, G. Ciardelli, Collagen for bone tissue regeneration, Acta Biomater. 8 (2012) 3191–3200, https://doi.org/10.1016/j.actbio.2012.06.014.

[9] S.A. Ghodbane, M.G. Dunn, Physical and mechanical properties of cross-linked type I collagen scaffolds derived from bovine, porcine, and ovine tendons, J. Biomed. Mater. Res. 104 (2016) 2685–2692, https://doi.org/10.1002/jbm.a.35813.

[10] J.E. Eastoe, The amino acid composition of mammalian collagen and gelatin, Biochem. J. 61 (1955) 589, https://doi.org/10.1042/bj0610589.

[11] A. Bonincontro, C. Mari, M. Mengoni, G. Risuleo, A study of the dielectric properties of E. coli ribosomal RNA and proteins in solution, Biophys. Chem. 67 (1997) 43–50, https://doi.org/10.1016/s0301-4622(97)00014-8.

[12] G.H. Bardelmeyer, Electrical conduction in hydrated collagen. I. Conductivity mechanism, Biopolymers 12 (1973) 2289–2302, https://doi.org/10.1002/bip.1973.360121008.

[13] M. Ashoorirad, M. Saviz, A. Fallah, On the electrical properties of collagen macromolecule solutions: role of collagen-water interactions, J. Mol. Liq. 300 (2020), 112344, https://doi.org/10.1016/j.molliq.2019.112344.

[14] F. Bibi, M. Villain, C. Guillaume, B. Sorli, N. Gontard, A review: origins of the dielectric properties of proteins and potential development as bio-sensors, Sensors 16 (2016) 1232, https://doi.org/10.3390/s16081232.

[15] M. Armand, F. Endres, D.R. MacFarlane, H. Ohno, B. Scrosati, Ionic-liquid materials for the electrochemical challenges of the future, Mater. Sustain. Energ. (2010) 129–137, https://doi.org/10.1142/9789814317665_0020.

[16] Z. Li, Z. Jia, Y. Luan, T. Mu, Ionic liquids for synthesis of inorganic nanomaterials, Curr. Opin. Solid State Mater. Sci. 12 (2008) 1–8, https://doi.org/10.1016/j.cossms.2009.01.002.

[17] A.P. Abbott, G. Capper, D.L. Davies, R.K. Rasheed, V. Tambyrajah, Quaternary ammonium zinc-or tin-containing ionic liquids: water insensitive, recyclable catalysts for Diels–Alder reactions, Green Chem. 4 (2002) 24–26, https://doi.org/10.1039/B108431C.

[18] T. Torimoto, T. Tsuda, K.C. Okazaki, S. Kuwabata, New frontiers in materials science opened by ionic liquids, Adv. Mater. 22 (2010) 1196–1221, https://doi.org/10.1002/adma.200902184.

[19] Z. Lei, B. Chen, Y.M. Koo, D.R. MacFarlane, Introduction: ionic liquids, Chem. Rev. 117 (2017) 6633–6635, https://doi.org/10.1021/acs.chemrev.7b00246.

[20] K. Ghandi, A review of ionic liquids, their limits and applications, Green Sustain. Chem. 4 (2014), 43349, https://doi.org/10.4236/gsc.2014.41008.

[21] T. Ueki, M. Watanabe, Macromolecules in ionic liquids: progress, challenges, and opportunities. Review, Macromolecules 41 (2008) 11, https://doi.org/10.1021/ma800171k.

[22] D.M. Correia, L.C. Fernandez, P.M.M. Martins, C. Garcia-Astrain, C.M. Costa, J. Reguera, S. Lanceros-Méndez, Ionic liquid-polymer composites: a new platform for multifunctional applications, Adv. Funct. Mater. 30 (2020), 1909736, https://doi.org/10.1002/adfm.201909736.

[23] A. Mehta, J. Rao, N.N. Fathima, Effect of ionic liquids on the different hierarchical order of collagen, Colloids Surf. B Biointerfaces 117 (2014) 376–382, https://doi.org/10.1016/j.colsurfb.2014.03.014.

[24] A. Tarannum, C. Muvva, A. Mehta, J.R. Rao, N.N. Fathima, Phosphonium based ionic liquids-stabilizing or destabilizing agents for collagen? RSC Adv. 6 (2016) 4022–4033, https://doi.org/10.1039/C5RA22441A.

[25] A. Tarannum, C. Muvva, A. Mehta, J. Raghava Rao, N.N. Fathima, Role of preferential ions of ammonium ionic liquid in destabilization of collagen, J. Phys. Chem. B 120 (2016) 6515–6524, https://doi.org/10.1021/acs.jpcb.6b02723.

[26] S.S. Silva, J.M. Gomes, L.C. Rodrigues, R.L. Reis, Marine-derived polymers in ionic liquids: architectures development and biomedical applications, Mar. Drugs 18 (2020) 346, https://doi.org/10.3390/md18070346.

[27] M. Reslan, V. Kayser, Ionic liquids as biocompatible stabilizers of proteins, Biophys. Rev. 10 (2018) 781–793, https://doi.org/10.1007/s12551-018-0407-6.

[28] M. Zahn, J. Föhles, M. Nlenhaus, A. Schwan, M. Spel, Ind. Eng. Chem. Prod. Res. Dev. 19 (1980) 496–501, https://doi.org/10.1021/i360076a005.

[29] A. Nuñez, R.A. Garcia, A. R, M. Aldema-Ramos, Characterizing wool keratin, Adv. Mater. Sci. Eng. (2009), 147175, https://doi.org/10.1155/2009/147175.

[30] J.G. Rouse, M.E. Van Dyke, A review of keratin-based biomaterials for biomedical applications, Materials 3 (2010) 999–1014, https://doi.org/10.3390/ma3020999.

[31] O. Väntsi, T. Kärki, Mineral wool waste in Europe: a review of mineral wool waste quantity, quality, and current recycling methods, J. Mater. Cycles Waste Manag. 16 (2014) 62–72, https://doi.org/10.1007/s10163-013-0170-5.

[32] S. Balaji, R. Kumar, R. Sripriya, U. Rao, A. Mandal, P. Kakkar, P.N. Reddy, P. K. Sehgal, Characterization of keratin-collagen 3D scaffold for biomedical application, Polym. Adv. Technol. 23 (2010) 500–507, https://doi.org/10.1002/pat.1905.

[33] Y. Ran, W. Su, L. Ma, Y. Tan, Z. Yi, X. Li, Developing exquisite collagen fibrillary assemblies in the presence of keratin nanoparticles for improved cellular affinity, Int. J. Biol. Macromol. 189 (2021) 380–390, https://doi.org/10.1016/j.ijbiomac.2021.08.134.

[34] R. Karthikeyan, S. Balaji, P.K. Sehgal, Industrial applications of keratins-A review, J. Sci. Ind. Res. 66 (2007) 710–715.

[35] N. Verma, M.K. Singh, S. Zafar, H. Pathak, Comparative study of in-situ temperature measurement during microwave-assisted compression-molding and conventionally compression-molding process, CIRP J. Manuf. Sci. Technol. 35 (2021) 336–345, https://doi.org/10.1016/j.cirpj.2021.07.005.

[36] L. Bozec, M. Odlyha, Thermal denaturation studies of collagen by microthermal analysis and atomic force microscopy, Biophys. J. 101 (2011) 228–236, https://doi.org/10.1016/j.bpj.2011.04.033.

[37] K. Tran-Ba, D.J. Lee, J. Zhu, K. Paeng, L.J. Kaufman, Confocal rheology probes the structure and mechanics of collagen through the sol-gel transition, Biophys. J. 113 (2017) 1882–1892, https://doi.org/10.1016/j.bpj.2017.08.025.

[38] K. Yoshimura, Y. Chonan, K. Shirai, Preparation and dynamic viscoelastic characterization of pepsin-solubilized collagen from shark skin compared with pig skin, Anim. Sci. J. 70 (1999) 227–234.

[39] Z. Tian, L. Duan, L. Wu, L. Shen, G. Li, Rheological properties of glutaraldehyde-crosslinked collagen analysed quantitatively using mechanical models, Mater. Sci. Eng. C 63 (2016) 10–17, https://doi.org/10.1016/j.msec.2016.02.047.

[40] C. Abeykoon, A. McMillan, C.H. Dasannayaka, X. Huang, P. Xu, Remanufacturing using end-of life vehicles and electrical and electronic equipment polymer recyclates - a paradigm for assessing the value proposition, Int. J. Lightweight Mater. Manuf. 4 (2021) 4344–4448, https://doi.org/10.1016/j.ijlmm.2021.06.005.

[41] B. Kaczmarek, A. Sionkowska, J. Skopinska-Wisniewska, Influence of glycosaminoglycans on the properties of thin films based on chitosan/collagen blends, J. Mech. Behav. Biomed. Mater. 80 (2018) 189–193, https://doi.org/10.1016/j.jmbbm.2018.02.006.

[42] V.I. Chakrapani, A. Gnanamani, V.R. Giridev, M. Madhusoothanan, G. Sekaran, Electrospinning of type I collagen and PCL nanofibers using acetic acid, J. Appl. Polym. Sci. 125 (2012) 3221–3227, https://doi.org/10.1002/app.36504.

[43] L. He, C. Mu, D. Li, W. Lin, Revisit the pre-transition of type I collagen denaturation in dilute solution by ultrasensitive differential scanning calorimetry, Thermochim. Acta 548 (2012) 1–5, https://doi.org/10.1016/j.tca.2012.08.024.

[44] m. Gauza-Włodarczyk, L. Kubisz, S. Mielcarek, D. Włodarczyk, Comparison of thermal properties of fish collagen and bovine collagen in temperature range 298-670 K, Mater. Sci. Eng. C 80 (2017) 468–471, https://doi.org/10.1016/j.msec.2017.06.012.

[45] A. Rochdi, A.L. Foucat, J.P. Renou, Effect of thermal denaturation on water-collagen interactions: NMR relaxation and differential scanning calorimetry analysis, Biopolymers 50 (1999) 690–696, https://doi.org/10.1002/(SICI)1097-0282(199912)50:7<690::AID-BIP2>3.0.CO;2-P.

[46] A. Barth, C. Zscherp, What vibrations tell about proteins, Q. Rev. Biophys. 35 (2002) 369–430, https://doi.org/10.1017/S0033583502003815.

[47] T. Riaz, R. Zeeshan, F. Zarif, K. Ilyas, N. Muhammad, S.Z. Safi, A. Rahim, S.A. A. Rizvi, I. U Rehman, FTIR analysis of natural and synthetic collagen, Appl. Spectrosc. Rev. 53 (2018) 703–746, https://doi.org/10.1080/05704928.2018.1426595.

[48] A. Reizabal, D.M. Correia, C.M. Costa, L. Perez-Alvarez, J.L. Vilas-Vilela, S. Lanceros-Mendez, Silk fibroin bending actuators as an approach towards natural polymer based active materials, ACS Appl. Mater. Interfaces 11 (2019) 30197–30206, https://doi.org/10.1021/acsami.9b07533.

[49] J.M. Cardamone, A. Nuñez, R.A. Garcia, M. Aldema-Ramos, Characterizing wool keratin, Res. Lett. Mater. Sci. (2009), 147175, https://doi.org/10.1155/2009/147175.

[50] Y. Zou, L. Wang, P. Cai, P. Li, M. Zhang, Z. Sun, C. Sun, W. Xu, D. Wang, Effect of ultrasound assisted extraction on the physicochemical and functional properties of collagen from soft-shelled turtle calipash, Int. J. Biol. Macromol. 105 (2017) 1602–1610, https://doi.org/10.1016/j.ijbiomac.2017.03.011.

[51] G.A. Valencia, C.G. Luciano, R.V. Lourenço, A.M.Q.B. Bittante, P.J.A. Sobral, Morphological and physical properties of nano-biocomposite films base on collagen loaded with laponite, Food Packag. Shelf Life 19 (2019) 24–30, https://doi.org/10.1016/j.fpsl.2018.11.013.

[52] K. Wang, R. Li, J.H. Ma, Y.K. Jian, J.N. Che, Extracting keratin from wool by using L-cysteine, Green Chem. 18 (2016) 476–481, https://doi.org/10.1039/c5gc01254f.

[53] V.R. Sherman, W. Yang, M.A. Meyers, The materials science of collagen, J. Mech. Behav. Biomed. Mater. 52 (2015) 22–50, https://doi.org/10.1016/j.jmbbm.2015.05.023.

[54] M. Rahman, C.S. Brazel, Ionic liquids: new generation stable plasticizers for poly (vinyl chloride), Polym. Degrad. Stabil. 91 (2006) 3371–3382, https://doi.org/10.1016/j.polymdegradstab.2006.05.012.

[55] A. Shavandi, M.A. Ali, Keratin based thermoplastic biocomposites: a review, Rev. Environ. Sci. Biotechnol. 18 (2019) 299–316, https://doi.org/10.1007/s11157-019-09497-x.

[56] X. Wu, A. Liu, W. Wang, R. Ye, Improve mechanical properties and thermal-stability of collagen fiber based film by crosslinking with casein, keratin or SPI: effect of crosslinking process and concentrations of proteins, Int. J. Biol. Macromol. 109 (2018) 1319–1328, https://doi.org/10.1016/j.ijbiomac.2017.11.144.
[57] M. Jachowicz, Electrostatic properties of selected personal protective equipment regarding explosion hazard, J. Sustain. Min. 12 (2013) 27–33, https://doi.org/10.7424/jsm130106.
[58] J.H. Christie, I.M. Woodhead, S. Krenek, J.R. Seocole, A new model of DC conductivity of hygroscopic solids: Part II: wool and silk, Textil. Res. J. 4 (2002) 303–308, https://doi.org/10.1177/004051750207200405.
[59] M. Ashoorirad, M. Saviz, A. Fallah, On the electrical properties of collagen macromolecule solutions: role of collagen-water interactions, J. Mol. Liq. 300 (2020), 112344, https://doi.org/10.1016/j.molliq.2019.112344.
[60] A. Tarannum, A. Adams, B. Blümich, N.N. Fathima, Impact of ionic liquids on the structure and dynamics of collagen, J. Phys. Chem. B 122 (2018) 1060–1065, https://doi.org/10.1021/acs.jpcb.7b09626.